

HIGHLY EFFICIENT SELF-ADAPTIVE REWARD SHAPING FOR REINFORCEMENT LEARNING

Anonymous authors

Paper under double-blind review

ABSTRACT

Reward shaping is a technique in reinforcement learning that addresses the sparse-reward problem by providing frequent and informative rewards. We introduce a self-adaptive and highly-efficient reward shaping mechanism that incorporates success rates derived from historical experiences as shaped rewards. The success rates are sampled from Beta distributions, which dynamically evolve from uncertain to reliable values as data accumulates. Initially, the shaped rewards exhibit more randomness to encourage exploration, while over time, increasing certainty enhances exploitation, naturally balancing exploration and exploitation. Our approach employs Kernel Density Estimation (KDE) with Random Fourier Features (RFF) to derive the Beta distributions, providing a computationally efficient and learning-free solution for high-dimensional state spaces. Our method is validated on various tasks with extremely sparse rewards, demonstrating notable improvements in sample efficiency and convergence stability over relevant baselines.

1 INTRODUCTION

Environments with extremely sparse rewards present notable challenges for reinforcement learning (RL). In such contexts, as the reward model lacks immediate signals, agents receive feedback only after long horizons, making the ability to quickly discover beneficial samples crucial for successful learning (Ladosz et al., 2022). To address this, a straightforward solution is to reconstruct the reward models by introducing auxiliary signals to assess the agent’s behavior, which has led to the popular technique of Reward Shaping (RS) (Strehl & Littman, 2008; Gupta et al., 2022). Inverse reinforcement learning (IRL), which extracts reward functions from human knowledge or expert demonstrations, represents an intuitive approach within this framework Arora & Doshi (2021). However, IRL heavily relies on extensive human input, which can be difficult to obtain especially in complex environments. Alternatively, fully autonomous approaches have emerged as an attractive direction.

Automatically maintained reward shaping can be broadly categorized into two branches: intrinsic motivation-based rewards, which are task-agnostic, and inherent value-based rewards, which are typically task-specific. The former mainly introduces exploration bonuses to encourage agents to explore a wider range of states, commonly by rewarding novel or infrequently visited states (Burda et al., 2018; Ostrovski et al., 2017; Tang et al., 2017; Bellemare et al., 2016). While these methods effectively enhance exploration, they tend to overlook the internal values of the states. This can lead to the “noisy TV” problem, where agents fixate on highly novel but meaningless regions, thus trapping them in suboptimal behaviors (Mavor-Parker et al., 2022). In contrast, the latter leverages high-level heuristics to guide agents in extracting meaningful values from learning experiences, which helps stabilize convergence. However, they often struggle in early exploration as non-directional guidance is involved (Ma et al., 2024; Memarian et al., 2021; Trott et al., 2019).

To overcome the limitations of existing RS methods and combine the advantages of exploration-encouraged and inherent value-based rewards, this paper introduces a novel **Self-Adaptive Success Rate** based reward shaping mechanism (**SASR**). The success rate, defined as the ratio of a state’s presence in successful trajectories to its total occurrences, works as an auxiliary reward distilled from historical experience. This success rate assesses a state’s contribution toward successful task completion, which closely aligns with the agent’s original objectives, offering informative guidance for learning. Furthermore, to mitigate overconfidence caused by deterministic success rates, we adopt Beta distributions to model success rates from a probabilistic perspective. Beta distributions

enable a self-adaptive evolution of confidence in approximating a state’s success rate, ensuring the system gradually converges to reliable rewards as more data is collected, while preventing premature certainty. To derive Beta distributions, we use kernel density estimation (KDE) enhanced by random Fourier features (RFF) to estimate success and failure counts, formulating a highly efficient approach. The main contributions of this paper are summarized as follows:

- We propose SASR, an autonomous reward-shaping mechanism designed for sparse-reward environments. By deriving a success rate from historical experiences that aligns with the agent’s optimization objectives, SASR effectively augments the environmental rewards.
- A novel self-adaptive mechanism is introduced to achieve an efficient exploration-exploitation balance. Initially, low-confidence Beta distributions provide uncertain rewards to expand the exploration range by perturbing the reward function and assigning higher rewards to unvisited states. As more experience accumulates, high-confidence Beta distributions offer more reliable and precise rewards to enhance exploitation.
- To derive the Beta distributions in continuous state spaces, we implement KDE with RFF, forming a learning-free approach that eliminates the need for additional neural networks or models, achieving remarkably low computational complexity.
- SASR is evaluated on various extremely sparse-reward tasks, significantly outperforming several baselines in sample efficiency, learning speed, and convergence stability.

2 RELATED WORK

Reward shaping (RS) methods can generally be categorized based on the source of learning: either from *human knowledge* or *agent’s own experiences*. Techniques that derive reward models from human knowledge, such as Inverse Reinforcement Learning (IRL) (Arora & Doshi, 2021; Ramachandran & Amir, 2007; Ziebart et al., 2008; Hadfield-Menell et al., 2016) and Inverse Optimal Control (IOC) (Schultheis et al., 2021), aim to extract reward or objective functions from expert demonstrations. Following this, transferring the learned reward models to new tasks has received considerable efforts (Biyik et al., 2022; Wu et al., 2021; Ellis et al., 2021; Cheng et al., 2021; Adamczyk et al., 2023; Lyu et al., 2024). However, these methods rely heavily on human-generated data and often struggle to adapt to out-of-distribution scenarios. Thus, our focus shifts toward autonomous self-learning approaches, which can be further divided into *intrinsic motivation-based* and *inherent value-based* rewards based on the nature of the rewards.

Intrinsic motivation based RS explores general heuristics or task-agnostic metrics to encourage exploration. Potential-based algorithms define the shaped reward as $\gamma\Phi(s') - \Phi(s)$, where $\Phi(\cdot)$ is a potential function. This ensures the reward cancels out in the Bellman equation, preserving the optimal policy (Devlin & Kudenko, 2012; Asmuth et al., 2008; Wiewiora, 2003). However, designing the potential function is highly dependent on the environmental dynamics, making it more applicable to model-based RL. More commonly, methods incorporate exploration bonuses to reward novel states (Mahankali et al., 2024; Devidze et al., 2022; Badia et al., 2020; Hong et al., 2018; Eysenbach et al., 2019). Representatively, count-based strategies track visitation counts and assign higher rewards to less frequently visited states (Lobel et al., 2023; Machado et al., 2020; Fox et al., 2018; Fu et al., 2017; Martin et al., 2017). In continuous spaces, state counting is challenging, so Tang et al. (2017) introduced a hash function to discretize the state space, Bellemare et al. (2016) proposed pseudo-counts based on recording probabilities, and Ostrovski et al. (2017) used PixelCNN Van den Oord et al. (2016). Additionally, random network distillation based methods measure state novelty by neural networks (Yang et al., 2024b; Burda et al., 2018), curiosity-driven approaches reward agents for encountering surprising or unpredictable states (Yang et al., 2024a; Sun et al., 2022; Burda et al., 2019; Pathak et al., 2017). Although intrinsic motivation has proven effective in enhancing exploration, only considering novelty while ignoring the inherent values of states may lead to suboptimal policies. A notable example illustrating this limitation is the “noisy TV” problem (Mavor-Parker et al., 2022), where agents may become attracted to irrelevant, dynamic stimuli that generate high novelty but provide no useful information.

Inherent value based RS, on the other hand, focuses on task-related signals that highlight how states contribute to achieving higher rewards and their underlying significance. For instance, Trott et al. (2019) introduced additional rewards based on the distance between a state and the target; Stadie et al. (2020) derived informative reward structures using a Self-Tuning Network to optimize

108 guidance; Memarian et al. (2021) captured the preferences among different trajectories by ranking
 109 them via a trained classifier; Zheng et al. (2018) minimized the KL-divergence between learned and
 110 original rewards to align their distributions. Mguni et al. (2023) used an auxiliary agent competing
 111 against the original agent in a Markov game; Instead, Ma et al. (2024) introduced ReLara, a col-
 112 laborative framework where an assistant reward agent automatically generates rewards to guide the
 113 policy agent. Moreover, incorporating multiple agents or hierarchical structures to share and trans-
 114 fer knowledge through synchronized reward functions is another promising research direction (Park
 115 et al., 2023; Yi et al., 2022; Gupta et al., 2023; Hu et al., 2020; Raileanu & Rocktäschel, 2020).

116 While intrinsic motivation rewards guide exploration, inherent value rewards support convergence,
 117 Ma et al. (2024) combined these two advances by introducing a scheme that evolves the shaped re-
 118 wards from random perturbations into meaningful metrics. Building on this idea, our study considers
 119 the success rate as an informative value. Compared with ReLara, which depends on a black-box RL
 120 agent and iterative optimization via backpropagation to achieve a well-performing reward model,
 121 our approach computes the shaped rewards directly from historical data, effectively reducing the
 122 delay of reward model convergence and enhancing explainability.

123 3 PRELIMINARIES

124 **Reinforcement Learning (RL)** aims to train an agent to interact with an environment, which is
 125 commonly modeled as a **Markov Decision Process (MDP)**. An MDP represented as $\langle S, A, T, R, \gamma \rangle$,
 126 involves four main components: S is the state space, A is the action space, $T : S \times A \times S \rightarrow [0, 1]$
 127 is the probability of transitioning from one state to another given a specific action, and $R : S \rightarrow \mathbb{R}$
 128 is the reward model. The objective in RL is to learn a policy $\pi(a|s)$ that maximizes the expected
 129 cumulative rewards $G = \mathbb{E}[\sum_{t=0}^{\infty} \gamma^t R(s_t)]$, where $\pi(a|s)$ indicates the likelihood of selecting action
 130 a in state s , and γ is the discount factor (Sutton & Barto, 2018).

131 **Beta Distribution** is defined on the interval $[0, 1]$, making it ideal for modeling proportions or
 132 probabilities. It is parameterized by α and β , which are interpreted as prior counts of successes and
 133 failures of a binary outcome. The probability density function of a Beta-distributed variable X is:

$$134 f(x; \alpha, \beta) = \frac{1}{B(\alpha, \beta)} x^{\alpha-1} (1-x)^{\beta-1}, \quad (1)$$

135 where $B(\alpha, \beta)$ is beta function. The key attribute of Beta distribution is its adaptability: as more data
 136 accumulates, the values of α and β increase, the distribution’s shape becomes narrower, thereby in-
 137 creasing confidence in the estimated probabilities. This feature is particularly beneficial in adaptive
 138 online learning, aligning closely with our objective of balancing exploration and exploitation.

139 **Kernel Density Estimation (KDE)** is a non-parametric approach to approximate the probability
 140 density function of a random variable from data samples. Given n data points $\{x_i\}_{i=1}^n$, KDE
 141 smooths these points to approximate the density function as follows:

$$142 \hat{d}(x) = \frac{1}{nh} \sum_{i=1}^n K\left(\frac{x-x_i}{h}\right), \quad (2)$$

143 where h is the bandwidth, $K(\cdot)$ is a kernel function such as Gaussian kernel, Laplacian kernel, or
 144 Cauchy kernel. KDE is particularly useful in scenarios where the actual distribution is not well-
 145 defined or complex, such as continuous state spaces in our RL environments.

152 4 METHODOLOGY

153 We propose a **Self-Adaptive Success Rate** based reward shaping mechanism (SASR) to accelerate
 154 RL algorithms learning in extremely-sparse-reward environments. Figure 1 illustrates the principles
 155 of the SASR mechanism: The diagram consists of two parts representing the early and late learning
 156 stages. As experiences accumulate with learning progresses, the Beta distributions modeling the
 157 success rates evolve from being more stochastic to more deterministic. This autonomous adaption
 158 closely aligns with the agent’s exploration-exploitation balance. Section 4.1 introduces how Beta
 159 distributions evolve and how shaped rewards are generated from them. Additionally, to achieve
 160 highly efficient computation, we leverage KDE and RFF to estimate success and failure counts,
 161

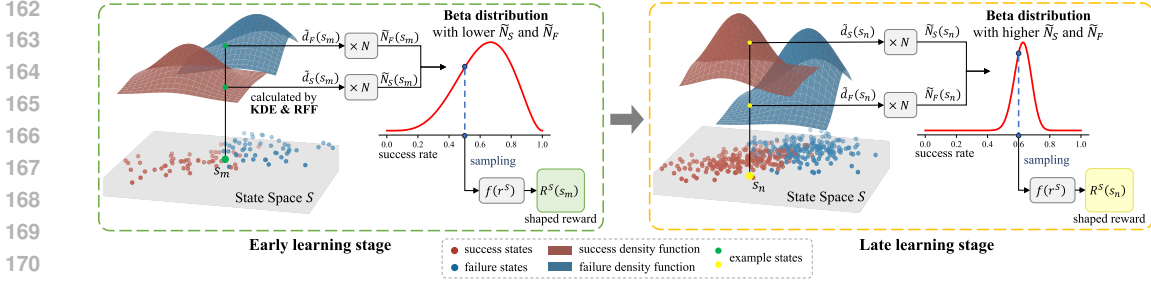


Figure 1: A schematic diagram of the self-adaptive success rate based reward shaping mechanism. KDE: Kernel Density Estimation; RFF: Random Fourier Features.

which are used to derive the corresponding Beta distributions, as detailed in Section 4.2. Lastly, Section 4.3 presents the integration of SASR into the RL agent and the overall algorithmic flow.

4.1 SELF-ADAPTIVE SUCCESS RATE SAMPLING

We formulate the augmented reward function in SASR as adding an auxiliary shaped reward $R^S(s)$ to the environmental reward $R^E(s)$, weighting by a factor λ :

$$R^{SASR}(s) = R^E(s) + \lambda R^S(s). \quad (3)$$

We assign the shaped reward $R^S(s_i)$ of a given state based on its *success rate* – defined as the ratio of the state’s presence in successful trajectories to its total occurrences. This metric provides a meaningful reward from a statistical perspective: a higher success rate, reflected in a higher shaped reward, indicates a greater likelihood that the state will guide the agent toward successful task completion. Formally, the **success rate based shaped reward** $R^S(s_i)$ is given by:

$$R^S(s_i) = f\left(\frac{N_S(s_i)}{N_S(s_i) + N_F(s_i)}\right), \quad (4)$$

where $N_S(s_i)$ and $N_F(s_i)$ denote the counts of state s_i appearing in successful and failed historical trajectories, respectively. To enhance scalability and adaptability, $f(\cdot)$ is a linear scaling function that maps the original success rate from $[0, 1]$ to a desired scale $[R_{min}, R_{max}]$, making the magnitude of the shaped rewards more flexible, i.e., $f(x) = R_{min} + x \cdot (R_{max} - R_{min})$.

Given $N_S(s_i)$ and $N_F(s_i)$, directly using a deterministic success rate may lead to overconfidence in the estimation of the true value. To address this, inspired by the principles of Thompson sampling (Thompson, 1933; Agrawal & Goyal, 2012), we adopt a probabilistic perspective for success rate estimation. Specifically, the success rate of each state is approximated as a variable in a Beta distribution, with shape parameters set as $\alpha = N_S(s_i) + 1$ and $\beta = N_F(s_i) + 1$:

$$r_i^S \sim \text{Beta}(r; \alpha, \beta) = \frac{1}{B(N_S(s_i) + 1, N_F(s_i) + 1)} r^{N_S(s_i)} (1 - r)^{N_F(s_i)}, \quad (5)$$

where the *beta function* $B(\cdot, \cdot)$ is the normalization factor. By sampling from this distribution, we obtain a probabilistic estimate of the true success rate. This sampled value, r_i^S , is then processed through the scaling function $f(\cdot)$ to produce the shaped reward: $R^S(s_i) = f(r_i^S)$.

As $N_S(s_i)$ and $N_F(s_i)$ progressively increase throughout the learning process, they influence the shape and sampling variability of the Beta distribution. Generating the shaped reward from these evolving Beta distributions offers several advantages:

- **Encourage Exploration.** In the early phases, lower counts of $N_S(s_i)$ and $N_F(s_i)$ result in Beta distributions with higher variance, making the sampled rewards more stochastic. This can be viewed as a noisy perturbation of the reward function. Given that the environmental rewards are predominantly zero, this perturbation optimizes the agent in diverse directions with tiny steps, shifting the anchors from which the stochastic policy sampling actions. Meanwhile, early-visited states are likely to fail, leading to a decrease in their success rates, while unvisited states retain the initial Beta distribution $\text{Beta}(1, 1)$, which in turn receives relatively higher rewards. This mechanism drives the agent to explore novel regions, aligning with the principles of intrinsic motivation. (Supporting experimental results in Section 5.2.)

- **Enhance Exploitation.** In the late phases, as the counts $N_S(s_i)$ and $N_F(s_i)$ increase, the Beta distribution gradually sharpens, concentrating generated rewards closer to the true success rate. The certain reward signals with higher confidence highly support the agent’s exploitation, facilitating more efficient convergence towards optimal policies.
- **Consistent Optimization.** The peak of the Beta distribution, computed as $N_S(s_i)/(N_S(s_i) + N_F(s_i))$, directly equals to the success rate. Meanwhile, the expectation, $(N_S(s_i) + 1)/(N_S(s_i) + N_F(s_i) + 2)$, closely approximates the success rate. This ensures that, despite stochastic, the overall reward remains consistent with policy optimization.

4.2 HIGHLY EFFICIENT BETA DISTRIBUTION DERIVATION

In this section, we present how the success and failure counts, $N_S(s_i)$ and $N_F(s_i)$, are derived for the Beta distributions. To efficiently estimate these counts in high-dimensional, continuous, or infinite state spaces, we use Kernel Density Estimation (KDE) to approximate the densities of successes and failures from accumulated experience. Specifically, we maintain two buffers, \mathcal{D}_S and \mathcal{D}_F , to store the states in successful and failed trajectories, respectively. By treating these states as scattered data instances distributed across the state space, KDE estimates the density as:

$$\tilde{d}_X(s_i) = \frac{1}{|\mathcal{D}_X|} \sum_{j=1}^{|\mathcal{D}_X|} K(s_i - s_j), \quad X \in \{S, F\}, \quad (6)$$

where $K(\cdot)$ is the kernel function and $|\mathcal{D}_X|$ is the buffer size. We select Gaussian kernel in our implementation. The estimated density $\tilde{d}_X(s_i)$ approximates the likelihood of encountering state s_i in success or failure scenarios, providing a statistically sound basis for estimating $N_X(s_i)$. By multiplying $\tilde{d}_X(s_i)$ by the total number of observed states N , the count $\tilde{N}_X(s_i)$ is estimated as:

$$\tilde{N}_X(s_i) = N \times \tilde{d}_X(s_i) = \frac{N}{|\mathcal{D}_X|} \sum_{j=1}^{|\mathcal{D}_X|} \exp\left(-\frac{\|s_i - s_j\|^2}{2h^2}\right), \quad X \in \{S, F\}, \quad (7)$$

where h is a hyperparameter, the bandwidth of the Gaussian kernel.

We further integrate Random Fourier Features (RFF) (Rahimi & Recht, 2007) to reduce computational complexity, as calculating the Gaussian kernel can be expensive, especially in scenarios involving high-dimensional state spaces and large buffers. RFF approximates the kernel function of the original k -dimensional states through an inner product of M -dimensional randomized features:

$$K(s_i, s_j) \approx z(s_i)^T z(s_j), \quad z(s) = \sqrt{\frac{2}{M}} \cos(\mathbf{W}^T s + \mathbf{b}), \quad (8)$$

where $z(\cdot)$ is the RFF mapping function with $\mathbf{W} = [\mathbf{w}^{(1)}, \dots, \mathbf{w}^{(M)}] \in \mathbb{R}^{k \times M}$ and $\mathbf{b} = [b^{(1)}, \dots, b^{(M)}]^T \in \mathbb{R}^M$ randomly sampled from the following *spectral* distributions:

$$\mathbf{w}^{(m)} \sim \mathcal{N}(\mathbf{0}, \sigma^{-2} \mathbf{I}_k), \quad b^{(m)} \sim \text{Uniform}(0, 2\pi), \quad m = 1, \dots, M, \quad (9)$$

where \mathbf{I}_k is the $k \times k$ identity matrix. Equation 9 is applied for the Gaussian kernel, while different kernels and the detailed derivations of the RFF method are provided in Appendix A.1.

4.2.1 IMPLEMENTATION DETAILS

Retention Rate. We introduce a hyperparameter, the *retention rate* $\phi \in (0, 1]$, to regulate the volume and diversity of states stored in the buffers. Rather than storing all encountered states, we uniformly retain a specific portion of ϕ . The motivations behind this are: (1) adjacent states in one trajectory tend to be highly similar, especially those near the initial state are repetitive and uninformative, retaining a portion of states can skip redundant states and increase sample diversity; (2) using a lower retention rate in the early stage keeps N_S and N_F lower, resulting in broader Beta distributions and preventing premature overconfidence.

Defining Success and Failure. In tasks where sparse rewards are only given at the end of an episode to indicate task completion, the entire trajectory can be classified as either a success or failure based on the episodic reward. For tasks with sparse rewards that do not explicitly indicate task completion, we segment the trajectories by positive reward occurrences. Specifically, if a reward is obtained within a pre-defined maximum steps, the corresponding sub-sequence is classified as a success; otherwise, it is considered a failure.

Algorithm 1 Self-Adaptive Success Rate based Reward Shaping

Require: Environment \mathcal{E} and agent \mathcal{A} .
Require: Experience replay buffer \mathcal{D} .
Require: State buffers for success \mathcal{D}_S and failure \mathcal{D}_F .
Require: RFF mapping function $z: \mathbb{R}^k \rightarrow \mathbb{R}^M$. ▷ Sample W and b based on Equation 9

- 1: **for** each trajectory $\tau = \emptyset$ **do**
- 2: **for** each environmental step **do**
- 3: $(s_t, a_t, s_{t+1}, r_t^E) \leftarrow \text{CollectTransition}(\mathcal{E}, \mathcal{A})$ ▷ interact with the environment
- 4: $\mathcal{D} \leftarrow \mathcal{D} \cup \{(s_t, a_t, s_{t+1}, r_t^E)\}$ ▷ store the transition in the replay buffer
- 5: $\tau \leftarrow \tau \cup \{s_t\}$ ▷ record the state in the trajectory
- 6: **end for**
- 7: **if** trajectory is successful: $\mathcal{D}_S \leftarrow \mathcal{D}_S \cup \tau$ ▷ store the trajectory in the success buffer
- 8: **else:** $\mathcal{D}_F \leftarrow \mathcal{D}_F \cup \tau$ ▷ otherwise, store the trajectory in the failure buffer
- 9: **end for**
- 10: **for** each update step **do**
- 11: $\{(s_t, a_t, r_t^E, s_{t+1})_i\} \sim \mathcal{D}$ ▷ sample a batch of transitions from the replay buffer
- 12: $\tilde{N}_S = z(s_t)^T z(\mathcal{D}_S)$ ▷ estimate the success counts
- 13: $\tilde{N}_F = z(s_t)^T z(\mathcal{D}_F)$ ▷ estimate the failure counts
- 14: $r_t^S \sim \text{Beta}(r; \tilde{N}_S + 1, \tilde{N}_F + 1)$ ▷ sample the success rate from the Beta distribution
- 15: $r_t^{\text{SASR}} = r_t^E + \lambda f(r_t^S)$ ▷ compute the SASR reward
- 16: Update agent \mathcal{A} with $\{(s_t, a_t, r_t^{\text{SASR}}, s_{t+1})_i\}$
- 17: **end for**

4.2.2 TIME AND SPACE COMPLEXITY OF SASR

Suppose the buffer size of \mathcal{D}_X is D and the batch size is B per iteration, the computational complexity to compute the count N_X is $O(MDB)$, indicating linear complexity (detailed derivation in Appendix A.2). RFF transforms nonlinear kernel computations into linear vector operations, significantly speeding up computation by leveraging the vectorization capabilities of GPUs (Dongarra et al., 2014). This demonstrates its higher efficiency compared to methods that rely on network updates and inferences involving extensive nonlinear computations.

Given the retention rate ϕ , the space complexity of maintaining two buffers is $O(\phi T |s|)$, where T is the total iterations and $|s|$ is the size of a single state. Moreover, storage space can be significantly conserved by leveraging the existing replay buffer in off-policy RL algorithms, like SAC (Haarnoja et al., 2018a) and TD3 (Fujimoto et al., 2018). Specifically, we augment the replay buffer with a flag that marks each state as either a success (flag = 1) or failure (flag = 0). Thereby, we can efficiently manage space requirements at the cost of minimal overhead from indexing processing.

For supporting experimental results in time and space complexity, please refer to Appendix A.3.

4.3 THE SASR MECHANISM FOR RL AGENTS

Building upon the SASR reward, we employ the soft actor-critic (SAC) algorithm by Haarnoja et al. (2018a) as the foundation for our RL agent. Let Q_ψ be parameterized Q-network and π_θ be parameterized policy network. The Q-network can be optimized by the following loss function:

$$\mathcal{L}(\psi) = \left(Q_\psi(s_t, a_t) - (r_t^E + \lambda R^S(s_t) + \gamma Q_{\psi'}(s_{t+1}, a_{t+1})) \right)^2, \quad (10)$$

where $Q_{\psi'}$ is obtained from a secondary frozen target network to maintain a fixed objective (Mnih et al., 2015). It is worth noting that the environmental reward r_t^E is retrieved from the replay buffer. Conversely, the shaped reward $R^S(s_t)$ is computed in real-time using the most recently updated $N_S(s_t)$ and $N_F(s_t)$, thereby capturing the latest advancements in learning progress.

We optimize the policy network by maximizing the expected Q-value and the entropy of the policy $\mathcal{H}(\pi_\theta(\cdot|s_t))$, following Haarnoja et al. (2018b):

$$\mathcal{L}(\theta) = \mathbb{E}_{a_t \sim \pi_\theta(\cdot|s_t)} \left[-Q_\psi(s_t, a_t) + \log \pi_\theta(a_t|s_t) \right]. \quad (11)$$

The flow of the SAC-embedded SASR algorithm is summarized in Algorithm 1.

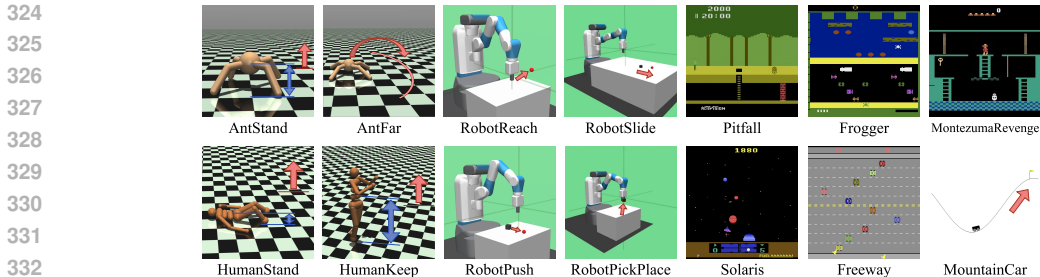


Figure 2: *MuJoCo*, robotic, *Atari* games and physical simulation tasks in our experiments. Detailed descriptions and the environmental reward models of each task are provided in Appendix A.8.

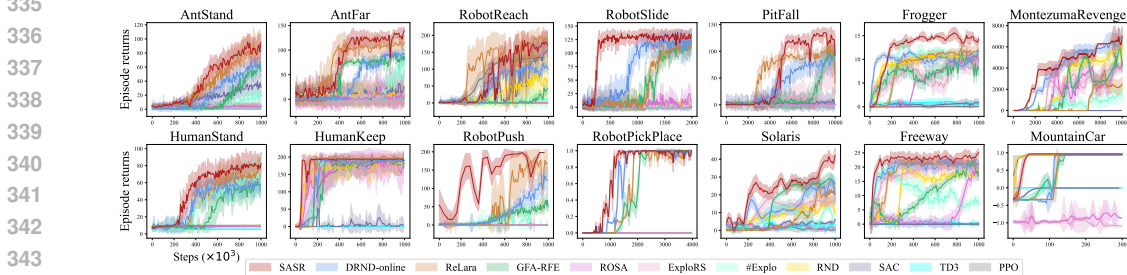


Figure 3: The learning performance of SASR compared with the baselines.

5 EXPERIMENTS

We evaluate SASR in high-dimensional environments, including four *MuJoCo* tasks (Todorov et al., 2012), four robotic tasks (de Lazcano et al., 2023), five *Atari* games, including the well-known *Montezuma’s Revenge* (Bellemare et al. (2013)), and a physical simulation task (Towers et al., 2023), as shown in Figure 2. All tasks provide extremely sparse rewards, with a reward of 1 granted only upon reaching the final objective within the maximum permitted steps. To ensure robust validation, we run 10 instances per setting with different random seeds and report average results. We also maintain consistent hyperparameters and network architectures across all tasks, detailed in Appendix A.8.

5.1 COMPARISON AND DISCUSSION

Baselines. We compare SASR with ten baselines to benchmark its performance: (a) the online Distributional Random Network Distillation (DRND) (Yang et al., 2024b), (b) RL with an Assistant Reward Agent (ReLara) (Ma et al., 2024), (c) General Function Approximation Reward-Free Exploration (GFA-RFE) (Zhang et al., 2024), (d) RL Optimizing Shaping Algorithm (ROSA) (Mguni et al., 2023), (e) Exploration-Guided RS (ExploRS) (Devidze et al., 2022), (f) Count-based static hashing exploration (#Explo) (Tang et al., 2017), (g) Random Network Distillation (RND) (Burda et al., 2018), (h) Soft Actor-Critic (SAC) (Haarnoja et al., 2018a), (i) Twin Delayed DDPG (TD3) (Fujimoto et al., 2018), and (j) Proximal Policy Optimization (PPO) (Schulman et al., 2017). Algorithms (a) to (g) are all reward shaping methods, involving either exploration bonuses or auxiliary agents to shape rewards, while algorithms (h) to (j) are advanced RL algorithms.

Figure 3 shows the learning performance of SASR compared with the baselines, and Table 1 reports the average episodic returns with standard errors achieved by the final models over 100 episodes. Our findings indicate that SASR surpasses the baselines in terms of sample efficiency, learning stability, and convergence speed. The primary challenge in these environments is the extremely sparse reward given after a long horizon, making exploration essential for timely obtaining successful trajectories. Although the exploration strategies of algorithms such as ExploRS, #Explo, and RND are designed to reward novel states, effectively expanding the early exploration space with the direct additional target, they continue focusing on discovering novel states, overlooking the implicit values of these states, which makes them fail to return to the final objectives.

SASR outperforms the baselines primarily due to its self-adaptive reward evolution mechanism. In the early phases, SASR encourages exploration by injecting substantial random rewards to optimize the agent in multiple directions, thereby increasing the likelihood of collecting positive samples.

Table 1: The average episodic returns and standard errors of all models tested over 100 episodes.

Tasks	SASR	DRND-online	ReLara	GFA-RFE	ROSA	ExploRS	#Explo	RND	SAC	TD3	PPO
AntStand	94.9±0.0	67.3±0.0	90.5±1.7	54.2±0.0	3.8±0.4	5.1±0.4	17.9±0.0	4.0±0.2	31.6±0.0	0.0±0.0	4.9±0.1
AntFar	139.8±0.0	93.2±0.0	115.7±0.0	86.4±0.0	1.0±0.0	12.0±4.2	75.1±0.0	4.6±1.6	25.3±0.0	1.0±0.0	7.8±0.0
HumanStand	79.8±2.0	50.6±0.0	76.2±0.7	58.2±0.0	8.8±0.0	9.3±0.0	72.7±0.0	9.3±0.1	9.9±0.0	5.5±0.0	9.0±0.1
HumanKeep	195.8±0.0	154.5±0.0	194.9±0.0	141.5±0.0	169.7±0.0	182.8±0.0	195.0±0.0	180.7±0.0	2.5±0.0	1.0±0.0	138.1±0.0
RobotReach	170.2±0.0	99.8±0.0	187.9±0.0	42.1±0.0	0.1±0.0	0.7±0.0	4.6±0.0	69.3±0.0	156.5±0.0	0.0±0.0	79.5±0.0
RobotSlide	132.3±1.3	127.2±0.0	111.6±2.0	115.8±2.0	11.2±0.9	4.3±0.1	3.5±0.0	4.8±0.2	0.7±0.2	0.5±0.4	0.2±0.2
RobotPush	167.1±0.0	122.2±0.0	166.9±0.0	49.1±0.0	0.0±0.0	0.0±0.0	3.7±0.0	0.0±0.0	0.0±0.0	0.0±0.0	0.0±0.0
RobotPickPlace	1.0±0.0	1.0±0.0	1.0±0.0	0.5±0.0	0.0±0.0	0.0±0.0	0.0±0.0	0.0±0.0	0.0±0.0	0.0±0.0	0.0±0.0
Pitfall	93.0±0.0	92.0±0.0	40.3±0.0	89.4±0.0	0.0±0.0	57.6±0.0	0.0±0.0	0.0±0.0	4.6±0.0	0.5±0.0	0.0±0.0
Frogger	14.2±0.0	11.7±0.0	11.6±0.0	7.9±0.0	9.8±0.0	8.3±0.0	11.9±0.0	10.5±0.0	0.8±0.0	0.7±0.0	0.0±0.0
Montezuma	6737.9±0.0	6828.5±0.0	2421.9±0.0	4755.3±0.0	4294.4±0.0	3971.5±0.0	1400.1±0.0	5494.3±0.0	0.0±0.0	0.0±0.0	0.0±0.0
Solaris	42.1±0.0	21.3±0.7	20.3±0.0	26.3±0.0	0.1±0.0	17.0±0.0	1.2±0.8	9.8±0.0	6.0±0.0	0.4±0.0	1.5±0.0
Freeway	22.4±0.0	19.8±0.0	21.5±0.0	10.1±0.0	18.0±0.0	17.5±0.0	6.9±0.0	13.0±0.0	0.1±0.0	0.2±0.0	0.0±0.0
MountainCar	1.0±0.0	1.0±0.0	1.0±0.0	1.0±0.0	-0.9±0.0	-1.0±0.0	1.0±0.0	1.0±0.0	-0.1±0.0	0.0±0.0	0.9±0.0

Moreover, almost all states are classified into the failure category, which leads to a decrease in the success rate of these states. Therefore, the unvisited states, which in turn receives relatively higher rewards, are encouraged to be visited. This mechanism is like the intrinsic motivation to give higher rewards to novel states, thus effectively guiding the agent to broaden the exploration space. As more data is collected, the success rate becomes more accurate, and the shaped reward provides more valuable guidance, significantly enhancing the exploitation and stabilizing the convergence toward optimal policies. Cooperatively, these strategies improve SASR’s sample efficiency and convergence stability in challenging tasks.

While ReLara used a similar exploration mechanism to SASR by perturbing reward functions, it relies on an independent black-box agent, requiring more iterations to converge. In contrast, SASR’s success rate sampling is more direct, reducing the delay in converging to valuable information. ReLara’s advantage lies in incorporating the policy agent’s actions into reward construction, as seen in the *RobotReach* task, where the target point is randomly selected in each episode. In this case, ReLara outperforms SASR due to access to action information. This can also be achieved in SASR by treating actions as additional features in the state vector.

5.2 EFFECT OF SELF-ADAPTIVE SUCCESS RATE SAMPLING

SASR introduces a novel self-adaptive mechanism that balances exploration and exploitation by maintaining the randomness of the shaped rewards. To further explore the effect of this mechanism, we use the *AntStand* task as a case study, analyzing the shaped rewards learned at different stages of training. Figure 4 (bottom) shows the learning curve, while Figure 4 (top) illustrates the distributions of generated rewards over the “height of the ant” feature, one dimension in the state vector.

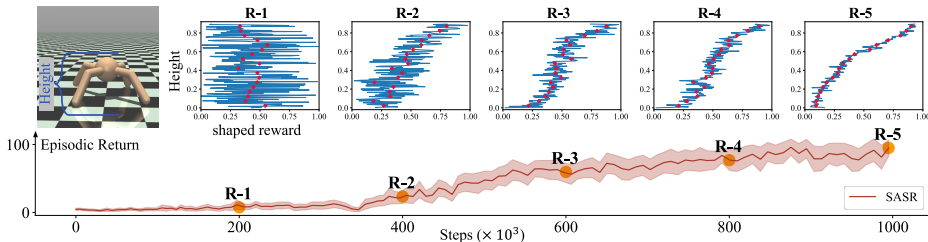


Figure 4: Distributions of the shaped rewards over the height of the ant robot in the *AntStand* task at different training stages. Red diamonds represent the estimated success rate, while the blue polylines show the actual shaped rewards sampled from the Beta distribution.

As learning progresses, the shaped rewards demonstrate two key attributes: the values transition from random to meaningful, and the variance decreases from uncertain to deterministic. Although the sampled rewards fluctuate, their center gradually shows a positive linear correlation with the robot’s height. In early phases, the shaped rewards contain significant randomness due to higher uncertainty. Although these random signals offer limited information, they drive the agent to take tiny optimization steps in diverse directions, effectively shifting the anchors of the policies, thus broadening the actions sampled from SAC’s stochastic policy, encouraging exploration, and increasing the diversity of collected samples. In later phases, the rewards converge to closely match the height of the robot, a meaningful and intuition-aligned metric, which enhances the agent’s exploitation.

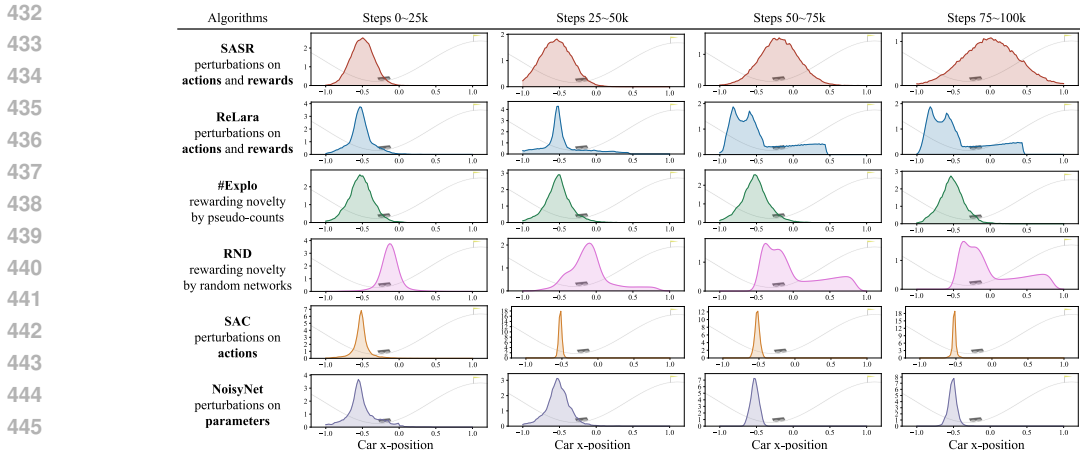


Figure 5: The density of visited states in the *MountainCar* task for four training periods.

To further investigate SASR’s exploration behavior, we compare the density of the visited states throughout the training in the *MountainCar* task with five representative exploration strategies: (1) ReLara, perturbing on both rewards and actions; (2) #Explo and (3) RND, rewarding novel states; (4) SAC, entropy-regularized exploration; and (5) NoisyNet (Fortunato et al., 2018), perturbing network weights. The density for every 25k steps is shown in Figure 5. We observe that SASR progressively covers a wider range of the state space. From 50k to 100k steps, SASR reaches positions near the goal, driven by the success rate mechanism. In contrast, ReLara and RND cover a similar range to SASR, but is less smooth and takes longer to reach the right side. #Explo shows no clear rightward shift, as it focuses on rewarding novelty, ignored the inherent value of states. SAC’s exploration is relatively narrow, making it easier to trap in local optima. NoisyNet shows a narrowing range as network weight perturbations diminish through optimization. Overall, SASR demonstrates more effective exploration and collects valuable samples sooner, leading to faster convergence.

5.3 ABLATION STUDY

We conduct ablation studies to investigate key components of SASR. We select six representative tasks to report the experimental results, and the quantitative data is provided in Appendix A.5.

Sampling from Beta distributions. (Figure 6a) We examine a variant of SASR that omits Beta distribution sampling, instead directly using the success rate $N_S(s_i)/(N_S(s_i) + N_F(s_i))$. In the early stages, limited experience makes this success rate an unreliable estimate, and using this fixed, overly confident value can mislead the agent. Furthermore, skipping Beta distribution sampling removes the exploration driven by random rewards, leading to narrower exploration. The results highlight the critical role of Beta distribution sampling for effective learning.

Reward function over state-action pair. (Figure 6b) We compare the performance of SASR with the reward function defined over the state-action pair, $r(s, a)$, and the state-only reward function, $r(s)$. The results show that both settings achieve similar performance levels. Encoding action into reward function increases the dimensionality, complicating density estimation and correlation assessment. Furthermore, the state and action vectors may exhibit different distributions, potentially reducing the accuracy of KDE estimations.

Retention rate ϕ . (Figure 6c) The retention rate controls the estimation of counts, which affects the confidence of Beta distributions. A high retention rate ($\phi = 1$) preserves all samples, resulting in a densely populated and redundant state pool, causing the Beta distribution to be prematurely overconfident, which degrades performance. Conversely, a low retention rate ($\phi = 0.01$) slows convergence by requiring more iterations to gather sufficient samples. The results suggest that an appropriate retention rate is important.

RFF feature dimensions M . (Figure 6d) SASR shows relatively low sensitivity to M , provided it is large enough to capture the states’ complexity. Results show that values like $M = 500, 1000, 2000$

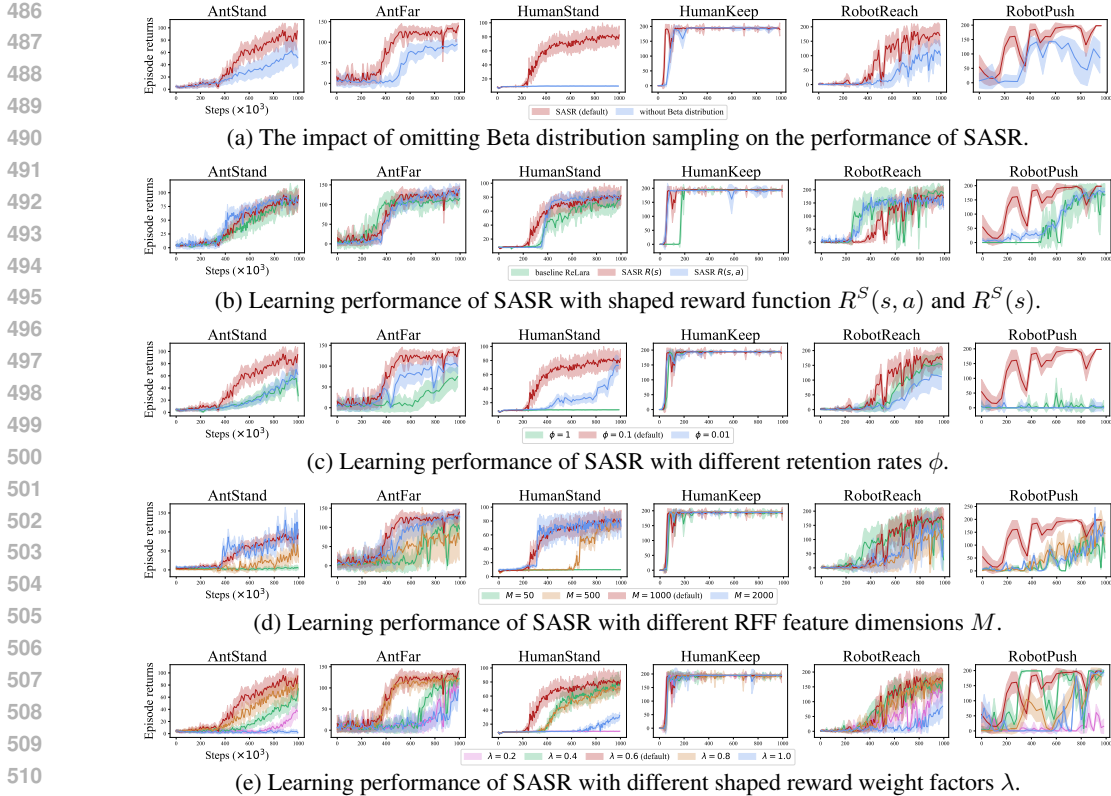


Figure 6: Ablation study: the impact of key components on the performance of SASR.

all yield similar performance levels, while significantly low dimensions, such as $M = 50$, degrade performance. This is also suggested in the original RFF study (Rahimi & Recht, 2007).

Shaped reward weight factor λ . (Figure 6e) Regarding the shaped reward weight factor λ , we observe that SASR performs better with intermediate values like $\lambda = 0.4, 0.6, 0.8$. At $\lambda = 0.2$, the minimal shaped reward scale reduces state differentiation, leading to suboptimal performance. At $\lambda = 1$, aligning the shaped reward scale with the environmental reward introduces excessive uncertainty and randomness, which may overwhelm the feedback and hinder learning. The findings highlight that maintaining a balanced reward scale is important for optimal learning outcomes.

6 CONCLUSION AND DISCUSSION

In this paper, we propose SASR, a self-adaptive reward shaping algorithm based on success rates, to address the sparse-reward challenge. SASR achieves an exploration and exploitation balance mechanism by generating shaped rewards from evolving Beta distributions. Experiments demonstrate that this adaptability significantly enhances the agent’s convergence speed. Additionally, the implementation of KDE and RFF formulates a highly-efficient and learning-free approach to deriving Beta distributions. This mechanism also provides a sound alternative to traditional count-based RS strategies, adapting effectively to continuous environments. Our evaluations confirm the superior performance of SASR in terms of sample efficiency and learning stability.

While SASR is designed for sparse-reward environments, in settings with dense rewards, the introduction and maintenance of additional shaped rewards could be unnecessary. Exploring the extension of SASR to dense reward scenarios presents a promising direction for further research. Moreover, the derivation of Beta distributions depends heavily on the samples stored in the success and failure buffers. Currently, our method does not account for the relationships or varying importance of different states within the same trajectory, making the algorithm sensitive to the retention rate ϕ . Therefore, developing an adaptive retention rate or better mechanisms for managing the buffers are crucial avenues for future improvement.

REFERENCES

- 540
541
542 Jacob Adamczyk, Argenis Arriojas, Stas Tiomkin, and Rahul V Kulkarni. Utilizing prior solutions
543 for reward shaping and composition in entropy-regularized reinforcement learning. In *Proceed-*
544 *ings of the AAAI Conference on Artificial Intelligence*, pp. 6658–6665, 2023.
- 545 Shipra Agrawal and Navin Goyal. Analysis of thompson sampling for the multi-armed bandit prob-
546 lem. In *Conference on learning theory*, pp. 39–1. JMLR Workshop and Conference Proceedings,
547 2012.
- 548 Saurabh Arora and Prashant Doshi. A survey of inverse reinforcement learning: Challenges, meth-
549 ods and progress. *Artificial Intelligence*, 297:103500, 2021.
- 550 John Asmuth, Michael L Littman, and Robert Zinkov. Potential-based shaping in model-based
551 reinforcement learning. In *AAAI Conference on Artificial Intelligence*, pp. 604–609, 2008.
- 552
553 Adrià Puigdomènech Badia, Pablo Sprechmann, Alex Vitvitskiy, Daniel Guo, Bilal Piot, Steven
554 Kapturowski, Olivier Tieleman, Martin Arjovsky, Alexander Pritzel, Andrew Bolt, et al. Never
555 give up: Learning directed exploration strategies. In *International Conference on Learning Rep-*
556 *resentations*, 2020.
- 557 Marc Bellemare, Sriram Srinivasan, Georg Ostrovski, Tom Schaul, David Saxton, and Remi Munos.
558 Unifying count-based exploration and intrinsic motivation. *Advances in Neural Information Pro-*
559 *cessing Systems*, 29, 2016.
- 560 Marc G Bellemare, Yavar Naddaf, Joel Veness, and Michael Bowling. The arcade learning environ-
561 ment: An evaluation platform for general agents. *Journal of Artificial Intelligence Research*, 47:
562 253–279, 2013.
- 563 Erdem Bıyık, Dylan P Losey, Malayandi Palan, Nicholas C Landolfi, Gleb Shevchuk, and Dorsa
564 Sadigh. Learning reward functions from diverse sources of human feedback: Optimally inte-
565 grating demonstrations and preferences. *The International Journal of Robotics Research*, 41(1):
566 45–67, 2022.
- 567 Yuri Burda, Harrison Edwards, Amos Storkey, and Oleg Klimov. Exploration by random network
568 distillation. In *International Conference on Learning Representations*, 2018.
- 569 Yuri Burda, Harri Edwards, Deepak Pathak, Amos Storkey, Trevor Darrell, and Alexei A Efros.
570 Large-scale study of curiosity-driven learning. In *International Conference on Learning Repre-*
571 *sentations*, 2019.
- 572 Ching-An Cheng, Andrey Kolobov, and Adith Swaminathan. Heuristic-guided reinforcement learn-
573 ing. *Advances in Neural Information Processing Systems*, 34:13550–13563, 2021.
- 574 Rodrigo de Lazcano, Kallinteris Andreas, Jun Jet Tai, Seungjae Ryan Lee, and Jordan
575 Terry. Gymnasium robotics, 2023. URL [http://github.com/Farama-Foundation/
576 Gymnasium-Robotics](http://github.com/Farama-Foundation/Gymnasium-Robotics).
- 577 Rati Devidze, Parameswaran Kamalaruban, and Adish Singla. Exploration-guided reward shaping
578 for reinforcement learning under sparse rewards. *Advances in Neural Information Processing
579 Systems*, 35:5829–5842, 2022.
- 580 Sam Michael Devlin and Daniel Kudenko. Dynamic potential-based reward shaping. In *Proceedings
581 of the 11th International Conference on Autonomous Agents and Multiagent Systems*, pp. 433–
582 440. IFAAMAS, 2012.
- 583 Jack Dongarra, Mark Gates, Azzam Haidar, Jakub Kurzak, Piotr Luszczek, Stanimire Tomov, and
584 Ichitaro Yamazaki. Accelerating numerical dense linear algebra calculations with gpus. *Numerical
585 computations with GPUs*, pp. 3–28, 2014.
- 586 Christian Ellis, Maggie Wigness, John Rogers, Craig Lennon, and Lance Fiondella. Risk averse
587 bayesian reward learning for autonomous navigation from human demonstration. In *IEEE/RSJ
588 International Conference on Intelligent Robots and Systems*, pp. 8928–8935. IEEE, 2021.

- 594 Benjamin Eysenbach, Abhishek Gupta, Julian Ibarz, and Sergey Levine. Diversity is all you need:
595 Learning skills without a reward function. In *International Conference on Learning Representations*,
596 2019.
- 597
598 Meire Fortunato, Mohammad Gheshlaghi Azar, Bilal Piot, Jacob Menick, Matteo Hessel, Ian Os-
599 band, Alex Graves, Volodymyr Mnih, Remi Munos, Demis Hassabis, Olivier Pietquin, Charles
600 Blundell, and Shane Legg. Noisy networks for exploration. In *International Conference on*
601 *Learning Representations*, 2018.
- 602 Lior Fox, Leshem Choshen, and Yonatan Loewenstein. Dora the explorer: Directed outreaching
603 reinforcement action-selection. In *International Conference on Learning Representations*, 2018.
- 604
605 Justin Fu, John Co-Reyes, and Sergey Levine. Ex2: Exploration with exemplar models for deep
606 reinforcement learning. *Advances in neural information processing systems*, 30, 2017.
- 607
608 Scott Fujimoto, Herke Hoof, and David Meger. Addressing function approximation error in actor-
609 critic methods. In *International Conference on Machine Learning*, pp. 1587–1596. PMLR, 2018.
- 610
611 Abhishek Gupta, Aldo Pacchiano, Yuexiang Zhai, Sham Kakade, and Sergey Levine. Unpacking re-
612 ward shaping: Understanding the benefits of reward engineering on sample complexity. *Advances*
613 *in Neural Information Processing Systems*, 35:15281–15295, 2022.
- 614
615 Dhawal Gupta, Yash Chandak, Scott Jordan, Philip S Thomas, and Bruno C da Silva. Behavior
616 alignment via reward function optimization. *Advances in Neural Information Processing Systems*,
36, 2023.
- 617
618 Tuomas Haarnoja, Aurick Zhou, Pieter Abbeel, and Sergey Levine. Soft actor-critic: Off-policy
619 maximum entropy deep reinforcement learning with a stochastic actor. In *International Confer-*
620 *ence on Machine Learning*, pp. 1861–1870. PMLR, 2018a.
- 621
622 Tuomas Haarnoja, Aurick Zhou, Kristian Hartikainen, George Tucker, Sehoon Ha, Jie Tan, Vikash
623 Kumar, Henry Zhu, Abhishek Gupta, Pieter Abbeel, et al. Soft actor-critic algorithms and appli-
cations. *arXiv preprint arXiv:1812.05905*, 2018b.
- 624
625 Dylan Hadfield-Menell, Stuart J Russell, Pieter Abbeel, and Anca Dragan. Cooperative inverse
626 reinforcement learning. *Advances in Neural Information Processing Systems*, 29, 2016.
- 627
628 Zhang-Wei Hong, Tzu-Yun Shann, Shih-Yang Su, Yi-Hsiang Chang, Tsu-Jui Fu, and Chun-Yi Lee.
629 Diversity-driven exploration strategy for deep reinforcement learning. *Advances in neural infor-*
mation processing systems, 31, 2018.
- 630
631 Yujing Hu, Weixun Wang, Hangtian Jia, Yixiang Wang, Yingfeng Chen, Jianye Hao, Feng Wu, and
632 Changjie Fan. Learning to utilize shaping rewards: A new approach of reward shaping. *Advances*
633 *in Neural Information Processing Systems*, 33:15931–15941, 2020.
- 634
635 Pawel Ladosz, Lilian Weng, Minwoo Kim, and Hyondong Oh. Exploration in deep reinforcement
learning: A survey. *Information Fusion*, 85:1–22, 2022.
- 636
637 Sam Lobel, Akhil Bagaria, and George Konidaris. Flipping coins to estimate pseudocounts for
638 exploration in reinforcement learning. In *International Conference on Machine Learning*, pp.
22594–22613. PMLR, 2023.
- 639
640 Jiafei Lyu, Xiaoteng Ma, Le Wan, Runze Liu, Xiu Li, and Zongqing Lu. Seabo: A simple search-
641 based method for offline imitation learning. 2024.
- 642
643 Haozhe Ma, Kuankuan Sima, Thanh Vinh Vo, Di Fu, and Tze-Yun Leong. Reward shaping for
644 reinforcement learning with an assistant reward agent. In *Forty-first International Conference on*
645 *Machine Learning*, volume 235, pp. 33925–33939. PMLR, 2024.
- 646
647 Marlos C Machado, Marc G Bellemare, and Michael Bowling. Count-based exploration with the
successor representation. In *Proceedings of the AAAI Conference on Artificial Intelligence*, pp.
5125–5133, 2020.

- 648 Srinath Mahankali, Zhang-Wei Hong, Ayush Sekhari, Alexander Rakhlin, and Pulkit Agrawal. Ran-
649 dom latent exploration for deep reinforcement learning. *International Conference on Machine*
650 *Learning*, 2024.
- 651
- 652 Jarryd Martin, S Suraj Narayanan, Tom Everitt, and Marcus Hutter. Count-based exploration in fea-
653 ture space for reinforcement learning. In *Proceedings of the 26th International Joint Conference*
654 *on Artificial Intelligence*, pp. 2471–2478, 2017.
- 655 Augustine Mavor-Parker, Kimberly Young, Caswell Barry, and Lewis Griffin. How to stay curious
656 while avoiding noisy tvs using aleatoric uncertainty estimation. In *International Conference on*
657 *Machine Learning*, pp. 15220–15240. PMLR, 2022.
- 658
- 659 Farzan Memarian, Wonjoon Goo, Rudolf Lioutikov, Scott Niekum, and Ufuk Topcu. Self-supervised
660 online reward shaping in sparse-reward environments. In *IEEE/RSJ International Conference on*
661 *Intelligent Robots and Systems*, pp. 2369–2375. IEEE, 2021.
- 662 David Mguni, Taher Jafferjee, Jianhong Wang, Nicolas Perez-Nieves, Wenbin Song, Feifei Tong,
663 Matthew Taylor, Tianpei Yang, Zipeng Dai, Hui Chen, et al. Learning to shape rewards using a
664 game of two partners. In *AAAI Conference on Artificial Intelligence*, pp. 11604–11612, 2023.
- 665
- 666 Volodymyr Mnih, Koray Kavukcuoglu, David Silver, Andrei A Rusu, Joel Veness, Marc G Belle-
667 mare, Alex Graves, Martin Riedmiller, Andreas K Fidjeland, Georg Ostrovski, et al. Human-level
668 control through deep reinforcement learning. *Nature*, 518(7540):529–533, 2015.
- 669 Georg Ostrovski, Marc G Bellemare, Aäron Oord, and Rémi Munos. Count-based exploration with
670 neural density models. In *International Conference on Machine Learning*, pp. 2721–2730. PMLR,
671 2017.
- 672
- 673 Seohong Park, Kimin Lee, Youngwoon Lee, and Pieter Abbeel. Controllability-aware unsupervised
674 skill discovery. In *International Conference on Machine Learning*, pp. 27225–27245. PMLR,
675 2023.
- 676
- 677 Deepak Pathak, Pulkit Agrawal, Alexei A Efros, and Trevor Darrell. Curiosity-driven exploration
678 by self-supervised prediction. In *International Conference on Machine Learning*, pp. 2778–2787.
PMLR, 2017.
- 679
- 680 Ali Rahimi and Benjamin Recht. Random features for large-scale kernel machines. *Advances in*
681 *neural information processing systems*, 20, 2007.
- 682
- 683 Roberta Raileanu and Tim Rocktäschel. Ride: Rewarding impact-driven exploration for
684 procedurally-generated environments. In *International Conference on Learning Representations*,
2020.
- 685
- 686 Deepak Ramachandran and Eyal Amir. Bayesian inverse reinforcement learning. In *International*
687 *Joint Conference on Artificial Intelligence*, volume 7, pp. 2586–2591, 2007.
- 688
- 689 John Schulman, Filip Wolski, Prafulla Dhariwal, Alec Radford, and Oleg Klimov. Proximal policy
optimization algorithms. *arXiv preprint arXiv:1707.06347*, 2017.
- 690
- 691 Matthias Schultheis, Dominik Straub, and Constantin A Rothkopf. Inverse optimal control adapted
692 to the noise characteristics of the human sensorimotor system. *Advances in Neural Information*
693 *Processing Systems*, 34:9429–9442, 2021.
- 694
- 695 Bradley Stadie, Lunjun Zhang, and Jimmy Ba. Learning intrinsic rewards as a bi-level optimization
696 problem. In *Conference on Uncertainty in Artificial Intelligence*, pp. 111–120. PMLR, 2020.
- 697
- 698 Alexander L Strehl and Michael L Littman. An analysis of model-based interval estimation for
markov decision processes. *Journal of Computer and System Sciences*, 74(8):1309–1331, 2008.
- 699
- 700 Hao Sun, Lei Han, Rui Yang, Xiaoteng Ma, Jian Guo, and Bolei Zhou. Exploit reward shifting
701 in value-based deep-rl: Optimistic curiosity-based exploration and conservative exploitation via
linear reward shaping. *Advances in Neural Information Processing Systems*, 35:37719–37734,
2022.

- 702 Richard S Sutton and Andrew G Barto. *Reinforcement learning: An introduction*. MIT press, 2018.
703
- 704 Haoran Tang, Rein Houthoofd, Davis Foote, Adam Stooke, OpenAI Xi Chen, Yan Duan, John Schul-
705 man, Filip DeTurck, and Pieter Abbeel. # exploration: A study of count-based exploration for
706 deep reinforcement learning. *Advances in Neural Information Processing Systems*, 30, 2017.
- 707 William R Thompson. On the likelihood that one unknown probability exceeds another in view of
708 the evidence of two samples. *Biometrika*, 25(3-4):285–294, 1933.
709
- 710 Emanuel Todorov, Tom Erez, and Yuval Tassa. Mujoco: A physics engine for model-based control.
711 In *IEEE/RSJ International Conference on Intelligent Robots and Systems*, pp. 5026–5033. IEEE,
712 2012.
- 713 Mark Towers, Jordan K. Terry, Ariel Kwiatkowski, John U. Balis, Gianluca de Cola, Tristan Deleu,
714 Manuel Goulão, Andreas Kallinteris, Arjun KG, Markus Krimmel, Rodrigo Perez-Vicente, An-
715 drea Pierré, Sander Schulhoff, Jun Jet Tai, Andrew Tan Jin Shen, and Omar G. Younis. Gymna-
716 sium, March 2023. URL <https://zenodo.org/record/8127025>.
- 717 Alexander Trott, Stephan Zheng, Caiming Xiong, and Richard Socher. Keeping your distance:
718 Solving sparse reward tasks using self-balancing shaped rewards. *Advances in Neural Information
719 Processing Systems*, 32, 2019.
720
- 721 Aaron Van den Oord, Nal Kalchbrenner, Lasse Espeholt, Oriol Vinyals, Alex Graves, et al. Con-
722 ditional image generation with pixellcn decoders. *Advances in neural information processing
723 systems*, 29, 2016.
- 724 Eric Wiewiora. Potential-based shaping and q-value initialization are equivalent. *Journal of Artificial
725 Intelligence Research*, 19:205–208, 2003.
726
- 727 Rand R Wilcox. *Introduction to robust estimation and hypothesis testing*. Academic press, 2011.
728
- 729 Yuchen Wu, Melissa Mozifian, and Florian Shkurti. Shaping rewards for reinforcement learning
730 with imperfect demonstrations using generative models. In *IEEE International Conference on
731 Robotics and Automation*, pp. 6628–6634. IEEE, 2021.
- 732 Kai Yang, Zhirui Fang, Xiu Li, and Jian Tao. Cmbe: Curiosity-driven model-based exploration
733 for multi-agent reinforcement learning in sparse reward settings. In *2024 International Joint
734 Conference on Neural Networks (IJCNN)*, pp. 1–8. IEEE, 2024a.
- 735 Kai Yang, Jian Tao, Jiafei Lyu, and Xiu Li. Exploration and anti-exploration with distributional ran-
736 dom network distillation. In *Forty-first International Conference on Machine Learning*. PMLR,
737 2024b.
738
- 739 Yuxuan Yi, Ge Li, Yaowei Wang, and Zongqing Lu. Learning to share in networked multi-agent
740 reinforcement learning. *Advances in Neural Information Processing Systems*, 35:15119–15131,
741 2022.
- 742 Junkai Zhang, Weitong Zhang, Dongruo Zhou, and Quanquan Gu. Uncertainty-aware reward-free
743 exploration with general function approximation. *International Conference on Machine Learning*,
744 2024.
745
- 746 Zeyu Zheng, Junhyuk Oh, and Satinder Singh. On learning intrinsic rewards for policy gradient
747 methods. *Advances in Neural Information Processing Systems*, 31, 2018.
- 748 Brian D Ziebart, Andrew L Maas, J Andrew Bagnell, Anind K Dey, et al. Maximum entropy inverse
749 reinforcement learning. In *AAAI Conference on Artificial Intelligence*, volume 8, pp. 1433–1438.
750 Chicago, IL, USA, 2008.
751
752
753
754
755

756 A APPENDIX

757 A.1 DERIVATION OF RANDOM FOURIER FEATURES

758 We incorporate Random Fourier Features (RFF) (Rahimi & Recht, 2007) to approximate the kernel
759 functions in the KDE process for the SASR algorithm. Let the original state be k -dimensional,
760 denoted as $\mathbf{s} \in \mathbb{R}^k$, and the kernel function be $k(\mathbf{s}_i, \mathbf{s}_j)$. RFF approximates the kernel function
761 by projecting the input k -dimensional space into a M -dimensional feature space using a mapping
762 function $z : \mathbb{R}^k \rightarrow \mathbb{R}^M$. The RFF-based kernel function is then defined as follows:
763

$$764 k(\mathbf{s}_i, \mathbf{s}_j) \approx z(\mathbf{s}_i)^T z(\mathbf{s}_j), \quad (12)$$

765 We provide the derivation of the RFF approximation in this section.

766 First, we clarify that RFF primarily targets shift-invariant kernels, that satisfy $k(\mathbf{s}_i, \mathbf{s}_j) = k(\mathbf{s}_i - \mathbf{s}_j)$.
767 Common shift-invariant kernels include Gaussian kernels, Laplacian kernels, and Cauchy kernels.
768 Given a shift-invariant kernel function $k(\Delta)$, we perform the inverse Fourier transform:
769

$$770 k(\mathbf{s}_i, \mathbf{s}_j) = \int_{\mathbb{R}^k} p(\mathbf{w}) e^{i\mathbf{w}^T(\mathbf{s}_i - \mathbf{s}_j)} d\mathbf{w} \quad (13)$$

$$771 = \mathbb{E}_{\mathbf{w}} [e^{i\mathbf{w}^T(\mathbf{s}_i - \mathbf{s}_j)}], \quad (14)$$

772 where we can consider $\mathbf{w} \sim p(\mathbf{w})$ based on the Bochner’s theorem, and $p(\mathbf{w})$ is called the *spectral*
773 *distribution* of kernel function. For the three types of shift-invariant kernels, the corresponding
774 spectral distributions are listed in Table 2:
775

776 Table 2: Some shift-invariant kernels and their associated spectral distributions.

Kernel	Kernel function, $k(\mathbf{s}_i - \mathbf{s}_j)$	Spectral density, $p(\mathbf{w})$
Gaussian	$\exp\left(-\frac{\ \mathbf{s}_i - \mathbf{s}_j\ _2^2}{h^2}\right)$	$\frac{\sqrt{h}}{2\sqrt{\pi}} \exp\left(-\frac{h\ \mathbf{w}\ _2^2}{4}\right)$
Laplacian	$\exp(-\ \mathbf{s}_i - \mathbf{s}_j\ _1)$	$\prod_{m=1}^M \frac{1}{\pi(1+w_d^2)}$
Cauchy	$\prod_{i=1}^k \frac{2}{\pi(1+(\mathbf{s}_i - \mathbf{s}_j)^2)}$	$\exp(-\ \mathbf{w}\ _1)$

777 Next, we perform the Euler’s formula transformation, which retains only the cosine term since we
778 are dealing with real-valued functions, the kernel function can be further derived as:
779

$$780 k(\mathbf{s}_i, \mathbf{s}_j) = \mathbb{E}_{\mathbf{w}} [e^{i\mathbf{w}^T(\mathbf{s}_i - \mathbf{s}_j)}] \quad (15)$$

$$781 = \mathbb{E}_{\mathbf{w}} [\cos(\mathbf{w}^T(\mathbf{s}_i - \mathbf{s}_j))] \quad (16)$$

$$782 = \mathbb{E}_{\mathbf{w}} [\cos(\mathbf{w}^T(\mathbf{s}_i - \mathbf{s}_j))] + \mathbb{E}_{\mathbf{w}} [\mathbb{E}_b[\cos(\mathbf{w}^T(\mathbf{s}_i + \mathbf{s}_j) + 2b)]] \quad (17)$$

$$783 = \mathbb{E}_{\mathbf{w}} [\mathbb{E}_b[\cos(\mathbf{w}^T(\mathbf{s}_i - \mathbf{s}_j)) + \cos(\mathbf{w}^T(\mathbf{s}_i + \mathbf{s}_j) + 2b)]] \quad (18)$$

$$784 = \mathbb{E}_{\mathbf{w}} [\mathbb{E}_b[\sqrt{2} \cos(\mathbf{w}^T \mathbf{s}_i + b) \sqrt{2} \cos(\mathbf{w}^T \mathbf{s}_j + b)]], \quad (19)$$

785 where $b \sim \text{Uniform}(0, 2\pi)$. Equation 17 holds since $\mathbb{E}_{b \sim \text{Uniform}(0, 2\pi)} [\cos(t + 2b)] = 0$ for any t .
786 Equation 19 is obtained from $\cos(A - B) + \cos(A + B) = 2 \cos(A) \cos(B)$, where $A = \mathbf{w}^T \mathbf{s}_i + b$,
787 $B = \mathbf{w}^T \mathbf{s}_j + b$.
788

789 We define the mapping $z_{\mathbf{w}, b}(\mathbf{s}) = \sqrt{2} \cos(\mathbf{w}^T \mathbf{s} + b)$, then the kernel function can be approxi-
790 mated by the inner product of two vectors and the expectation can be approximated by Monte Carlo
791 sampling:
792

$$793 k(\mathbf{s}_i, \mathbf{s}_j) = \mathbb{E}_{\mathbf{w}} [\mathbb{E}_b [z_{\mathbf{w}, b}(\mathbf{s}_i) z_{\mathbf{w}, b}(\mathbf{s}_j)]] \quad (20)$$

$$794 \approx \frac{1}{M} \sum_{m=1}^M z_{\mathbf{w}_d, b_d}(\mathbf{s}_i) z_{\mathbf{w}_d, b_d}(\mathbf{s}_j) \quad (21)$$

$$795 = z(\mathbf{s}_i)^T z(\mathbf{s}_j). \quad (22)$$

Therefore, we have derived the mapping function $z(\mathbf{s}) = \sqrt{2/M} \cos(\mathbf{W}^T \mathbf{s} + \mathbf{b})$, where $\mathbf{W} \in \mathbb{R}^{M \times k}$ and $\mathbf{b} \in \mathbb{R}^M$. The RFF-based kernel function can be approximated by the inner product of the mapped features in the M -dimensional space.

A.2 DERIVATION OF COMPUTATION COMPLEXITY

In this section, we derive the computational complexity to retrieve the success or failure counts N_S and N_F for each iteration. Suppose the buffer size of \mathcal{D}_X is D , the batch size of \mathcal{B} is B , the corresponding counts are retrieved by calculating:

$$\tilde{N}_X = N \times z(\mathcal{B})^T z(\mathcal{D}_X), \quad (23)$$

where the mapping function is defined as:

$$z(\mathbf{s}) = \sqrt{\frac{2}{M}} \cos(\mathbf{W}^T \mathbf{s} + \mathbf{b}), \quad \mathbf{W} \in \mathbb{R}^{k \times M}, \quad \mathbf{b} \in \mathbb{R}^M. \quad (24)$$

For each state, the mapping function calculation involves:

1. Matrix multiplication $\mathbf{W}^T \mathbf{s}$: kM .
2. Addition $\mathbf{W}^T \mathbf{s} + \mathbf{b}$: M .
3. Cosine calculation $\cos(\mathbf{W}^T \mathbf{s} + \mathbf{b})$: M .

Therefore, the computational complexity for calculating $z(\mathbf{s})$ for one state is $O(kM)$.

For each pair of states $(\mathbf{s}_i, \mathbf{s}_j)$, calculating the kernel involves M multiplications and $M - 1$ additions, thus, the complexity is $O(M)$.

For each iteration, we calculate the RFF mapping for all states in the buffer and the batch and then compute the kernel between them. The complexities involve three parts: RFF mapping for the buffer, RFF mapping for the batch and kernel calculation:

$$O(DkM) + O(BkM) + O(MDB). \quad (25)$$

Since the first two terms $O(DkM)$ and $O(BkM)$ are dominated by the last term $O(MDB)$ when the buffer size and the batch size are large, the overall computational complexity to retrieve the corresponding counts can be approximated as $O(MDB)$.

A.3 EXPERIMENTS ON TIME AND SPACE COMPLEXITY

A.3.1 TIME AND SPACE COMPLEXITY COMPARISON

In this section, we analyze the time and space overhead introduced by SASR and other representative reward-shaping methods. Below, we summarize the computational and memory costs of the RS baselines, introduced by the shaped reward generation.

- **SASR (ours)** calculates shaped rewards using RFF, which essentially is matrix operations, without additional networks/models learning processes. Regarding the memory costs, the buffers D_S and D_F are much smaller than the replay buffer used in the backbone SAC algorithm, due to the retention rate ϕ . While considering the scalability for larger problems, we have implemented an alternative approach by augmenting the original replay buffer in the backbone SAC algorithm with a success or failure flag. This approach avoids the need for additional buffers.
- **ReLara** (Ma et al., 2024) requires an additional RL agent (of the same scale as the original RL agent) and an additional replay buffer.
- **ROSA** (Mguni et al., 2023) involves a competition agent (the same scale as the original RL agent) and a switching model (a neural network).
- **ExploRS** (Devidze et al., 2022) requires learning two parameterized networks: one for a self-supervised reward model and another for the exploration bonus.
- **#Explo** (Tang et al., 2017) requires a hash function to discretize the state space and a hash table to store the state-visitation counts.
- **RND** (Burda et al., 2018) uses a random network distillation module to compute the intrinsic rewards.

Furthermore, we report the computational and memory costs of SASR and the RS baselines in two tasks: *AntStand* and *Frogger*, the results are shown in Table 3 and Table 4, respectively. To provide a more intuitive comparison, we report the relative value normalized to our SASR, in this case, if the value > 1 , it indicates that the baseline is more computationally or memory expensive than SASR, and vice versa.

Table 3: Average maximum memory consumption during the training process, normalized to SASR.

Tasks	<u>SASR</u>	ReLara	ROSA	ExploRS	#Explo	RND
<i>AntStand</i>	<u>1</u>	3.67	4.12	2.05	0.89	0.12
<i>Frogger</i>	<u>1</u>	5.21	4.33	2.64	0.92	0.09

Table 4: Average training time, normalized to SASR.

Tasks	<u>SASR</u>	ReLara	ROSA	ExploRS	#Explo	RND
<i>AntStand</i>	<u>1</u>	1.87	2.12	1.67	1.08	1.11
<i>Frogger</i>	<u>1</u>	1.98	3.17	1.72	1.24	1.06

A.3.2 COMPARISON OF SASR WITH AND WITHOUT RFF

To evaluate the effect of introducing RFF, we compare the training time of SASR with and without RFF, also with the backbone SAC algorithm, the results are shown in Table 5. The tests are conducted on the NVIDIA RTX A6000 GPU. The results show that excluding SAC’s inherent optimization time, RFF significantly saves time in the SASR algorithm, while with varying effects across tasks.

Table 5: Comparison of training time (in hours) for SASR with and without RFF.

Algorithms	<i>AntStand</i>	<i>AntFar</i>	<i>HumanStand</i>	<i>HumanKeep</i>	<i>RobotReach</i>	<i>RobotPush</i>
SAC (backbone)	5.87	5.08	4.87	5.67	5.42	6.3
SASR KDE+RFF	7.15	7.52	6.92	6.20	7.07	8.13
SASR w/o RFF	8.12	8.72	8.37	6.53	11.12	9.21

A.4 AUTO HYPERPARAMETER SELECTION

To improve the robustness and generalization of the SASR algorithm, we propose some potential autonomous hyperparameter selection strategies, mainly designed for the bandwidth h of the kernel function and the RFF feature dimension M .

For bandwidth h , we can use the empirical formula *Silverman’s Rule of Thumb* (Wilcox, 2011):

$$h = 1.06 \cdot \sigma \cdot N^{-1/5}, \quad (26)$$

or cross-validation to determine the optimal bandwidth.

For the RFF dimension M , it is directly related to the bandwidth h . After determining h , we can use the formula mentioned in the RFF theory to determine M :

$$M = O\left(\frac{1}{\epsilon^2} \log \frac{N}{\delta}\right), \quad (27)$$

where ϵ and δ are the error and confidence parameters. Another method is to compare the Frobenius norm error between the RFF approximated kernel matrix K^{RFF} and the true kernel matrix $K^{Gaussian}$ to select M : $\|K^{RFF} - K^{Gaussian}\|_F$.

Table 6: Ablation study #1: The average episodic returns and standard errors of SASR and the variant without sampling from Beta distributions.

Tasks	SASR (with sampling)	SASR (without sampling)
<i>AntStand</i>	94.92±0.00	54.48 ± 1.29
<i>AntFar</i>	139.84±0.00	92.77 ± 1.53
<i>HumanStand</i>	79.83±2.03	9.77 ± 0.02
<i>HumanKeep</i>	195.77±0.00	185.00 ± 0.00
<i>RobotReach</i>	170.18±0.00	110.29 ± 2.93
<i>RobotPush</i>	167.14±0.00	86.82 ± 0.00

Table 7: Ablation study #2: The average episodic returns and standard errors of SASR with reward function on state-action pair or state only.

Tasks	SASR (with $R^S(s)$)	SASR (with $R^S(s, a)$)
<i>AntStand</i>	94.92±0.00	85.61±1.30
<i>AntFar</i>	139.84±0.00	132.49±2.92
<i>HumanStand</i>	79.83±2.03	78.93±0.65
<i>HumanKeep</i>	195.77±0.00	192.54±0.16
<i>RobotReach</i>	170.18±0.00	151.95±5.74
<i>RobotPush</i>	167.14±0.00	179.76±1.66

Table 8: Ablation study #3: The average episodic returns and standard errors of SASR with different retention rates.

Tasks	$\phi = 1$	$\phi = 0.1$ (default)	$\phi = 0.01$
<i>AntStand</i>	45.71±7.57	94.92±0.00	62.85±3.49
<i>AntFar</i>	70.07±3.30	139.84±0.00	103.65±2.57
<i>HumanStand</i>	9.88±0.01	79.83±2.03	66.46±2.96
<i>HumanKeep</i>	195.00±0.00	195.77±0.00	194.77±0.10
<i>RobotReach</i>	154.32±0.89	170.18±0.00	112.46±0.90
<i>RobotPush</i>	2.96±1.97	167.14±0.00	1.75±1.24

Table 9: Ablation study #4: The average episodic returns and standard errors of SASR with different RFF feature dimensions M .

Tasks	$M = 50$	$M = 500$	$M = 1000$ (default)	$M = 2000$
<i>AntStand</i>	5.21±0.45	50.68±6.40	94.92±0.00	96.80±8.42
<i>AntFar</i>	98.88±2.64	72.17±5.07	139.84±0.00	129.87±0.63
<i>HumanStand</i>	9.87±0.01	78.82±0.52	79.83±2.03	77.73±1.47
<i>HumanKeep</i>	193.84±0.61	194.71±0.15	195.77±0.00	195.86±0.03
<i>RobotReach</i>	119.09±26.92	122.89±4.51	170.18±0.00	94.87±15.56
<i>RobotPush</i>	71.67±27.53	161.70±11.54	167.14±0.00	150.20±8.70

Table 10: Ablation study #5: The average episodic returns and standard errors of SASR with different shaped reward weight factors.

Tasks	$\lambda = 0.2$	$\lambda = 0.4$	$\lambda = 0.6$ (default)	$\lambda = 0.8$	$\lambda = 1.0$
<i>AntStand</i>	35.71±0.92	59.82±2.71	94.92±0.00	75.61±1.41	3.16±0.35
<i>AntFar</i>	99.83±3.25	119.82±1.18	139.84±0.00	119.35±1.80	80.71±4.74
<i>HumanStand</i>	9.81±0.02	75.35±1.06	79.83±2.03	70.96±0.51	28.94±0.46
<i>HumanKeep</i>	194.68±0.08	194.21±0.38	195.77±0.00	193.85±0.42	194.89±0.10
<i>RobotReach</i>	131.61±4.51	154.16±5.20	170.18±0.00	169.00±2.56	74.23±4.23
<i>RobotPush</i>	13.07±1.65	193.56±3.85	167.14±0.00	178.90±0.00	192.07±0.87

A.5 SUPPLEMENTARY EXPERIMENTAL RESULTS FOR ABLATION STUDY

In this section, we provide the detailed quantitative results of the ablation study.

Bandwidth h of Gaussian kernel. The bandwidth h controls the smoothness of the kernel functions. Beyond fixed bandwidths, we also test a linearly decreasing configuration ($h : 0.5 \rightarrow 0.1$), which reflects increasing confidence in KDE. Results indicate that a small bandwidth ($h = 0.01$) increases the distance between samples, causing many to have zero estimated density, while a large bandwidth ($h = 1$) makes samples indistinguishable due to an overly flat kernel function. Both cases result in suboptimal performance. The decreasing bandwidth setting offers no significant improvement and tends to reduce stability due to inconsistent density estimations.

Table 11: Ablation study #6: The average episodic returns and standard errors of SASR with different bandwidths h of Gaussian kernel.

Tasks	$h = 0.01$	$h = 0.1$	$h = 0.2$ (default)	$h = 1$	$h = 0.5 \rightarrow 0.1$
<i>AntStand</i>	10.71±2.52	57.22±3.87	94.92±0.00	17.74±2.53	68.40±1.54
<i>AntiFar</i>	17.58±2.84	99.80±4.41	139.84±0.00	25.83±8.62	136.49±4.15
<i>HumanStand</i>	9.89±0.01	64.47±1.87	79.83±2.03	9.90±0.02	58.79±2.76
<i>HumanKeep</i>	194.92±0.02	194.00±0.57	195.77±0.00	193.06±0.46	194.59±0.18
<i>RobotReach</i>	128.57±3.83	97.35±19.12	170.18±0.00	134.02±2.02	59.39±26.02
<i>RobotPush</i>	2.29±1.62	122.45±37.58	167.14±0.00	0.00±0.00	0.01±0.01

A.6 NETWORK STRUCTURES AND HYPERPARAMETERS

A.6.1 NETWORK STRUCTURES

Figure 7 illustrates the structures of the policy network and Q-network employed in our experiments. The agent utilizes simple multilayer perceptron (MLP) models for these networks. Given the use of stochastic policies, the policy network features separate heads to generate the means and standard deviations of the inferred normal distributions, which are then used to sample actions accordingly.

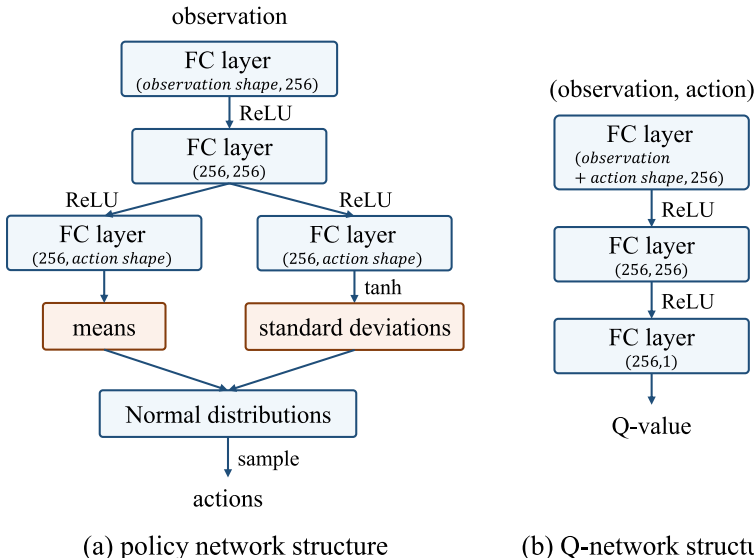


Figure 7: The structures of policy network and Q-network in our implementation.

A.6.2 HYPERPARAMETERS

We have observed that SASR demonstrated high robustness and was not sensitive to hyperparameter choices. Table 12 shows the set of hyperparameters that we used in all of our experiments.

Table 12: The hyperparameters used in the SASR algorithm.

Hyperparameters	Values
reward weight λ (default)	0.6
kernel function bandwidth	0.2
random Fourier features dimension M	1000
retention rate ϕ (default)	0.1
discounted factor γ	0.99
replay buffer size $ \mathcal{D} $	1×10^6
batch size	256
actor module learning rate	3×10^{-4}
critic module learning rate	1×10^{-3}
SAC entropy term factor α learning rate	1×10^{-4}
policy networks update frequency (steps)	2
target networks update frequency (steps)	1
target networks soft update weight τ	5×10^{-3}
burn-in steps	5000

A.7 COMPUTE RESOURCES

The experiments in this paper were conducted on a computing cluster, with the detailed hardware configurations listed in Table 13. The computing time for the SASR algorithm in each task (running 1,000,000 steps) was approximately 6 ± 2 hours.

Table 13: The compute resources used in the experiments

Component	Specification
Operating System (OS)	Ubuntu 20.04
Central Processing Unit (CPU)	2x Intel Xeon Gold 6326
Random Access Memory (RAM)	256GB
Graphics Processing Unit (GPU)	1x NVIDIA A100 20GB
Brand	Supermicro 2022

A.8 CONFIGURATIONS OF TASKS

In this section, we provide the detailed configurations of the tasks in the experiments.

- *AntStand*: The ant robot is trained to stand over a target position. The reward is given if the ant robot reaches the target height. Maximum episode length is 1000 steps.
- *AntFar*: The ant robot is trained to reach a target position far from the starting point. The reward is given if the ant robot reaches the target position. Maximum episode length is 1000 steps.
- *HumanStand*: The human robot is trained to stand over a target position. The robot is initialized by lying on the ground, and the reward is given if the robot reaches the target height. Maximum episode length is 1000 steps.
- *HumanKeep*: The human robot is trained to keep a target height. The robot is initialized by standing, and the reward is given if the robot maintains the target height. Maximum episode length is 1000 steps.
- *RobotReach*: The robot arm is trained to reach a target position. The target position is randomly generated in the workspace, and the reward is given if the robot reaches the target position. Maximum episode length is 500 steps.
- *RobotPush*: The robot arm is trained to push an object to a target position. The target position is randomly generated on the table, and the reward is given if the object reaches the target position. Maximum episode length is 500 steps.
- *RobotSlide*: The robot arm is trained to slide an object to a target position. The target position is randomly generated on the table, and the reward is given if the object reaches the target position. Maximum episode length is 500 steps.

- 1080 • *RobotPickPlace*: The robot arm is trained to pick and place an object to a target position. The
1081 target position is randomly generated in the space, and the reward is given if the object reaches
1082 the target position. Maximum episode length is 500 steps.
- 1083 • *Pitfall*: The agent is tasked with collecting all the treasures in a jungle while avoiding the pitfalls.
1084 The reward is given if the agent collects one treasure, while if the agent falls into a pitfall, the
1085 episode ends. Maximum episode length is 2000 steps.
- 1086 • *Froger*: The agent is trained to cross frogs on a river. The reward is given when each frog is
1087 crossed, and the episode ends if all frogs are crossed or fall into the river. Maximum episode
1088 length is 2000 steps.
- 1089 • *MontezumaRevenge*: The agent is trained to navigate through a series of rooms to collect keys
1090 and reach the final room. The reward is given if the agent successfully reaches one new room.
1091 Maximum episode length is 5000 steps.
- 1092 • *Solaris*: The agent controls a spaceship to blast enemies and explore new galaxies. The reward
1093 is given if the agent destroys one enemy spaceship and enters a new galaxy. Maximum episode
1094 length is 2000 steps.
- 1095 • *Freeway*: The agent is trained to guide the chicken across multiple lanes of heavy traffic. The
1096 reward is given if one chicken crosses one lane, while the episode ends if all chickens are crossed
1097 or hit by a car. Maximum episode length is 2000 steps.
- 1098 • *MountainCar*: The car is trained to reach the top of the right hill. The reward is given if the car
1099 reaches the top. Maximum episode length is 1000 steps.

1100 Furthermore, we provide the detailed dimensions of the states in our evaluated tasks in Table 14.

1101 Table 14: The dimensions of the states in the evaluated tasks.

Domain (Tasks)	Dimension
Ant robot (<i>AntStand</i> , <i>AntFar</i>)	105
Humanoid robot (<i>HumanStand</i> , <i>HumanKeep</i>)	348
<i>RobotReach</i>	20
<i>RobotPush</i> , <i>RobotSlide</i> and <i>RobotPickPlace</i>	35
Atari games (<i>MontezumaRevenge</i> , <i>PitFall</i> , <i>Frooger</i> , <i>Solaris</i> , <i>Freeway</i>)	$84 \times 84 = 7056$
<i>MountainCar</i>	2

1110
1111
1112
1113
1114
1115
1116
1117
1118
1119
1120
1121
1122
1123
1124
1125
1126
1127
1128
1129
1130
1131
1132
1133